Supplementary Material for "Flux states and topological phases from spontaneous time-reversal symmetry breaking in CrSi(Ge)Te_3-based systems"

(Dated: May 23, 2016)

I. PROJECTED DENSITY OF STATES AND ORBITAL CHARACTER

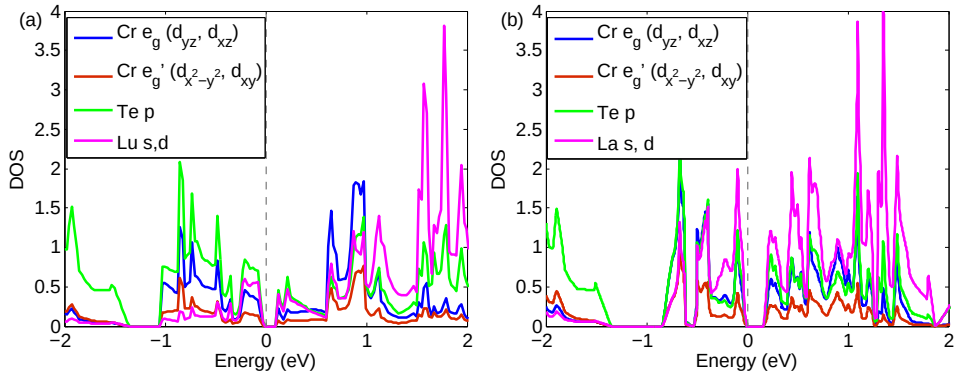

FIG. 1: Local density of states projected onto various orbitals in the majority-spin channel, (a) for 1 ML Lu deposited on single-layer $CrGeTe_3$, and (b) for 1 ML La deposited on single-layer $CrSiTe_3$. The Fermi level is at $E = 0$.

In this section, we make a detailed analysis of the orbital character of 1 mono-layer (ML) La deposited on single-layer (SL) $CrSiTe_3$ and 1 ML Lu deposited on SL $CrGeTe_3$. Following the convention introduced in the main text, we call these two systems "Si-La" and "Ge-Lu" for simplicity. We first review the electronic structure of bulk $CrSiTe_3$ ($CrGeTe_3$). In the ionic crystal picture, the on-site Coulomb repulsion between the Cr $3d$ electrons ($\sim$3.5 eV) pushes the $3d$ orbitals in the minority spin channel far above the Fermi level. The important physics of the system is thus dominated by the $3d$ orbitals in the majority spin channel. The five-fold degenerate majority-spin $3d$ orbitals are then split into a_{1g} (d_{z^2}), e_g (d_{yz} and d_{xz}) and e_g' ($d_{x^2-y^2}$ and d_{xy}) levels in the rhombohedral crystal field environment. The magnetic moment of $CrSiTe_3$ ($CrGeTe_3$) was reported to be ~ 2.73 (2.80) μ_B per Cr atom, [1, 2] suggesting that Cr is a 3+ cation in these compounds. The remaining three electrons on the Cr ion then occupy the majority-spin a_{1g} and e_g' orbitals, giving rise to $\sim 3\,\mu_B$ for each ion. We assume a 2− oxidation state for Te, with the Te p orbitals fully occupied and lying somewhat below the Fermi level. The four empty e_g states (from the two Cr sites) in the majority spin channel are located immediately above the Fermi level, leading to an indirect gap $\sim$0.4 eV for $CrSiTe_3$ as reported in Ref. 3.

If 1 ML La (Lu) is deposited on SL $CrSiTe_3$ ($CrGeTe_3$), the La (Lu) atom tends to donate two of its three valence electrons to the unoccupied Cr e_g (d_{yz} and d_{xz}) orbitals, making the four majority-spin e_g states half filled, while the remaining electron occupies the $5d$ or $6s$ orbitals of the adatom also in the majority-spin channel. Therefore, with adatoms deposited, there are five physically important states around the Fermi level, namely, the two occupied Cr e_g states, the one occupied s or d state from the adatom, and the two unoccupied Cr e_g states, all in the majority spin channel.

However, as discussed in the main text, $CrSiTe_3$ and $CrGeTe_3$ have a strongly covalent character, as the hybridization between Cr $3d$ and Te $4p$ orbitals is fairly strong. The above analysis based on the ionic crystal picture can be carried over, except that the states around the Fermi level no longer have simple orbital character. In Fig. 1 we show the local density of states (DOS) for the Ge-Lu (Fig. 1(a)) and Si-La (Fig. 1(b)) systems projected onto various atomic orbitals in the majority-spin channel. The states around the Fermi level have significant contributions from both Cr d and Te p orbitals, and the Lu (La) s and d orbitals also play important roles. It follows that the hybridization effects in these two systems are strong, so the influence of nonlocal Coulomb interactions is expected to be significant.

II. WANNIERIZED TIGHT-BINDING MODELS, SURFACE STATES, ANOMALOUS HALL CONDUCTIVITY, AND INTER-SITE CURRENTS

We use the Wannier90 code package [4, 5] to generate realistic tight-binding (TB) models for the Si-La and Ge-Lu systems. These TB models are "realistic" in the sense that the bandstructures from the TB models exactly reproduce those from first-principles calculations within an energy window that extends from $-1.5\,\mathrm{eV}$ below to $+1.5\,\mathrm{eV}$ above the Fermi level. The Bloch functions obtained from the first-principles calculations are projected onto Cr s, Cr d, Te p, Si (Ge) p, and La (Lu) s and d orbitals to construct the corresponding Wannier functions in each spin channel. Then one can extract the hopping parameters of the 42-band TB model in each spin channel for each system, and calculate various physical quantities using such TB models.

In order to calculate the edge states as shown in Fig. 5(a) and (c) in the main text, we truncate the Wannierized TB models in the (010) direction, and the semi-infinite spectral functions are calculated using the iterative Green's-function method reported in Ref. 6. The anomalous Hall conductivities shown in Fig. 5(b) and (d) of the main text are calculated using the Wannier-interpolation method proposed by Wang *et al.*[7]

The inter-site current is also calculated in the Wannier basis. The net current flowing onto site j can be expressed as

$$\begin{aligned}
\frac{dn_j}{dt} &= \mathrm{Tr}\Big[\frac{d\hat{n}_j}{dt}\,\hat{\rho}\Big] \\
&= \sum_{j',m}\langle W_{mj'}|\,\frac{i}{\hbar}[H,\hat{n}_j]\,\hat{\rho}\,|W_{mj'}\rangle \\
&= \frac{i}{\hbar}\sum_{m}\langle W_{mj}|\,[\hat{\rho},H]\,|W_{mj}\rangle \\
&= \frac{i}{\hbar}\sum_{j'}\sum_{m,m'}\left(\rho_{mj,m'j'}H_{m'j',mj}-H_{mj,m'j'}\rho_{m'j',mj}\right) \\
&= \sum_{j'}F_{j'j}\ , \qquad (1)
\end{aligned}$$

where j and j' run over atomic sites and m is the index of Wannier functions on each site, with $|W_{mj}\rangle$ representing the mth Wannier function located at site j. H is the Hamiltonian, and $\hat{n}_j = \sum_m |W_{mj}\rangle\langle W_{mj}|$ is the number operator on site j. $\hat{\rho}$ is the density operator; at zero temperature, $\hat{\rho}$ can be expressed in terms of the occupied Bloch states as $\hat{\rho} = A_0\int d^2k/(2\pi^2)\sum_n |\psi_{n\mathbf{k}}\rangle\langle\psi_{n\mathbf{k}}|\,\theta(\epsilon_f - \epsilon_{n\mathbf{k}})$, where $|\psi_{n\mathbf{k}}\rangle$ and $\epsilon_{n\mathbf{k}}$ are the Bloch state and the corresponding band energy, ϵ_f is the Fermi level ($\theta(x)=1$ for $x>0$, and $\theta(x)=0$ otherwise), and A_0 is the area of the primitive cell. $\rho_{mj,m'j'}$ and $H_{mj,m'j'}$ are the matrix elements of the density operator and the Hamiltonian in the Wannier basis. In the last line of Eq. (1), $F_{j'j} = (-2/\hbar)\sum_{m,m'}\mathrm{Im}[\rho_{mj,m'j'}H_{m'j',mj}]$ is interpreted as the current flowing between site j and j'.

III. ENERGY BANDS, ANOMALOUS HALL CONDUCTIVITIES, AND ORBITAL MOMENTS INCLUDING SPIN-ORBIT COUPLING

The spin-orbit-coupled bandstructures of Ge-Lu and Si-La are shown in Fig. 2(a) and (b) respectively. With spin-orbit coupling (SOC) included, the indirect gap for Ge-Lu decreases from $\sim$70 meV to $\sim$60 meV, while it increases from $\sim$130 meV to $\sim$160 meV for the Si-La system. The Chern numbers for both systems are +1. The anomalous Hall conductivities (σ_{yx}) for the Ge-Lu and Si-La systems are shown in Fig. 3(a) and Fig. 3(b) respectively. Clearly σ_{yx} in the gap is quantized at e^2/h for both systems. One may also notice that there is an abrupt sign change of σ_{yx} for the Ge-Lu system when the the Fermi level is placed in the conduction band. This results from the SOC-induced avoided crossings at $\sim$0.1 eV around K and $\sim$0.15 eV around $\overline{K}$ as shown in Fig. 2(a). Such avoided crossings would lead to peaks of Berry curvature with opposite signs around K and $\overline{K}$, which are not at the same energy due to broken TR symmetry. This gives rise to the abrupt sign change of σ_{yx} shown in Fig. 3(a).

If we assume that the directions of the spin moments are not reversed after including SOC, then the choice of the Chern number becomes unique due to SOC. In other words, one of the two otherwise

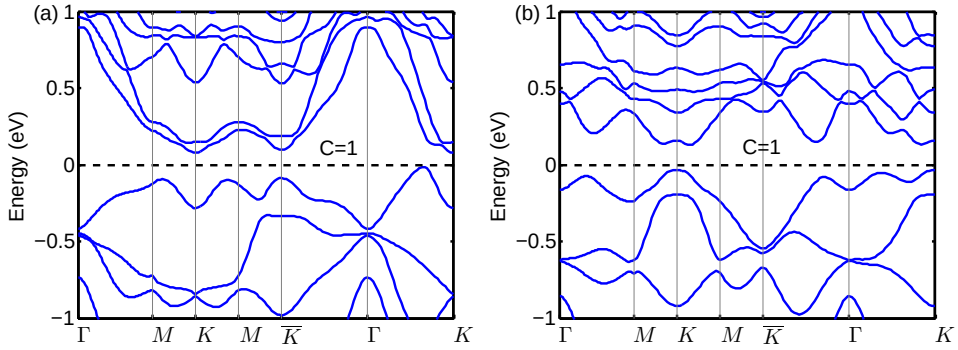

FIG. 2: Bandstructures when spin-orbit coupling is included, (a) for Ge-Lu, and (b) for Si-la. The Fermi levels are at $E = 0$.

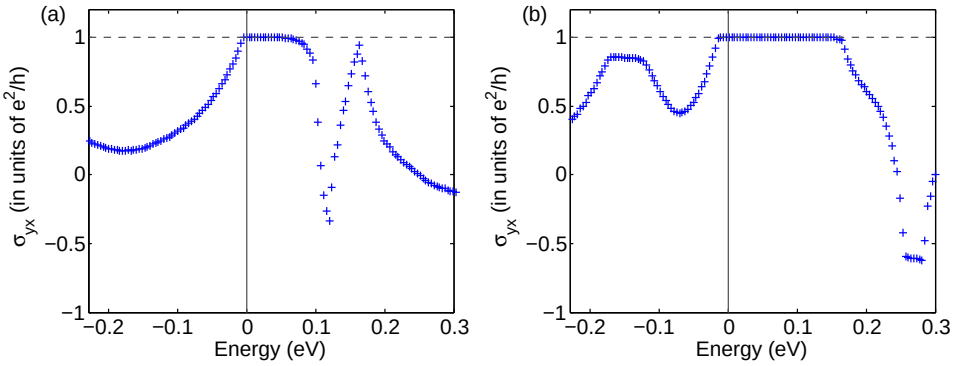

FIG. 3: The anomalous Hall conductivities including spin-orbit coupling for (a) Ge-Lu system, and (b) Si-La.

time-reversal-equivalent ground states with opposite Chern numbers becomes lower in energy. To be specific, we list the z components of the spin and orbital moments (denoted by M_S and M_L respectively) of different atomic sites for the two systems in the following two tables.

The spin and orbital moments for the Ge-Lu system are shown in Table I. When SOC is turned off, the ground state is a flux state with orbital moments $\{-0.126\,\mu_B,\, 0.113\,\mu_B\}$ for the two Cr sites, where the first moment refers to that of the adatom-covered Cr site. This is equivalent to the state with all the orbital moments flipped. When SOC is turned on, the two degenerate ground states become nondegenerate, and the orbital moments on the two Cr sites become $\{-0.120\,\mu_B,\, 0.115\,\mu_B\}$. Moreover, SOC tends to induce weak orbital moments on the three bottom Te sites, which sum to $0.018\,\mu_B$, and are parallel to the corresponding on-site spin moments (which sum to $0.291\,\mu_B$). As the p shell of a Te atom is more than half-filled, the orbital and spin moments tend to be parallel to maximize the energy gain from SOC according to Hund's third rule.

The spin and orbital moments for the Si-La system are listed in Table II. Without SOC, the reported orbital moments on the two Cr sites are $\{-0.066\,\mu_B,\, 0.082\,\mu_B\}$, and the orbital moment on the La site is $-0.180\,\mu_B$ and is associated with the La $5d$ electrons. Again, such a flux state is degenerate with its time-reversal (TR) partner with flipped orbital moments. When SOC is turned on, the signs of the orbital moments become reversed: the two Cr sites change from $\{-0.066\,\mu_B,\, 0.082\,\mu_B\}$ to $\{0.071\,\mu_B,\, -0.080\,\mu_B\}$, and the orbital moment on the La site changes from $-0.180\,\mu_B$

TABLE I: Spin and orbital moments for the Ge-Lu system, in μ_B.

		Cr1	Cr2	Ge dimer	bottom Te	top Te	Lu
Without SOC	M_S	−3.767	−3.755	−0.094	0.282	0.041	−0.253
	M_L	−0.126	0.113	0.001	0.004	−0.003	−0.016
With SOC	M_S	−3.771	−3.762	−0.093	0.291	0.044	−0.249
	M_L	−0.120	0.115	0.001	0.018	0.003	0.000

TABLE II: Spin and orbital moments for the Si-La system, in μ_B.

		Cr1	Cr2	Ge dimer	bottom Te	top Te	La
Without SOC	M_S	−3.804	−3.729	−0.084	0.374	0.178	−0.636
	M_L	−0.066	0.082	0.000	0.001	−0.003	−0.180
With SOC	M_S	−3.805	−3.728	−0.081	0.369	0.177	−0.644
	M_L	0.071	−0.080	0.000	0.015	0.006	0.294

to $0.294\,\mu_B$. This results from the fact that the La $5d$ shell is less than half filled, so that the energy gain from SOC is maximized if the La on-site orbital moment ($0.294\,\mu_B$) and spin moment ($-0.644\,\mu_B$) are anti-parallel. Since the SOC strength of La is much larger than that of Cr, the system tends to choose the state with anti-parallel spin and orbital moments on the La site.

IV. FLUX STATES WITH TRIVIAL BAND TOPOLOGY

As discussed in the main text, a flux state is not necessarily topologically nontrivial. For example, TR symmetry is broken in the majority-spin subspace in both 1 ML Lu deposited on SL $CrSiTe_3$ and 1 ML La deposited on SL $CrGeTe_3$ (denoted as "Si-Lu" and "Ge-La" for simplicity), and there are spontaneously generated current loops surrounding the Cr sites leading to antiferromagnetically ordered orbital moments. However, both of these systems are topologically trivial. Fig. 4(a) and (b) show the bandstructures in the absence of SOC for Si-Lu and Ge-La respectively. The blue (red) lines indicate the energy bands in the majority (minority) spin channel. It is straightforward to see that orbital TR symmetry is broken only in the majority spin channel, suggesting that the ground states of the systems are flux states. However, orbital-character analysis (not shown) indicates that there is no band inversion in these systems, and that their computed Chern numbers remain zero.

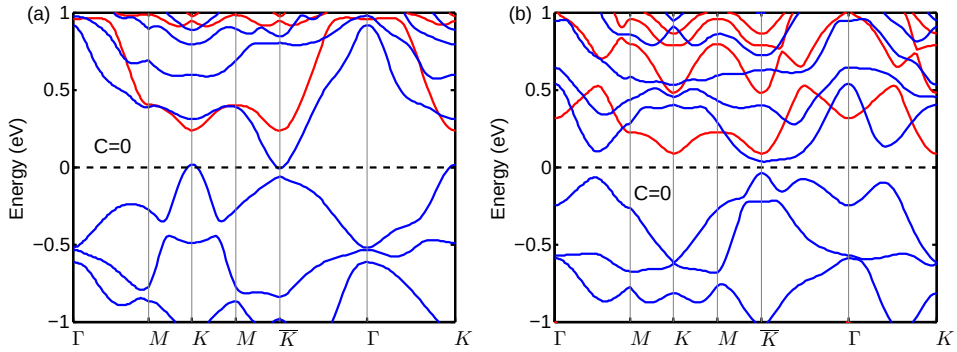

FIG. 4: Bandstructures for (a) 1 ML Lu deposited on single-layer $CrSiTe_3$, and (b) 1 ML La deposited on single-layer $CrGeTe_3$. The blue and red curves represent energy bands in the majority-spin and minority-spin channels.

[1] V. Carteaux, F. Moussa, and M. Spiesser, EPL (Europhysics Letters) **29**, 251 (1995).
[2] V. Carteaux, D. Brunet, G. Ouvrard, and G. Andre, Journal of Physics: Condensed Matter **7**, 69 (1995).
[3] L. Casto, A. Clune, M. Yokosuk, J. Musfeldt, T. Williams, H. Zhuang, M.-W. Lin, K. Xiao, R. Hennig, B. Sales, et al., APL Materials **3**, 041515 (2015).
[4] A. A. Mostofi, J. R. Yates, Y. S. Lee, I. Souza, D. Vanderbilt, and N. Marzari, Computer Phys. Comm. **178**, 685 (2008).
[5] N. Marzari, A. A. Mostofi, J. R. Yates, I. Souza, and D. Vanderbilt, Rev. Mod. Phys. **84**, 1419 (2012).
[6] M. L. Sancho, J. L. Sancho, J. L. Sancho, and J. Rubio, Journal of Physics F: Metal Physics **15**, 851 (1985).
[7] X. Wang, J. R. Yates, I. Souza, and D. Vanderbilt, Phys. Rev. B **74**, 195118 (2006).